Maximise absorbed wave power with wave energy converter arrays in time domain

KARA, Fuat

Maximise absorbed wave power with wave energy converter arrays in time domain

Fuat Kara
Sheffield Hallam University, S1 1WB, fuat.kara@shu.ac.uk

Abstract

A three-dimensional transient numerical code ITU-WAVE based on potential theory and Neumann-Kelvin approximation is extended to take into account wave interaction in an array system using two and four truncated vertical cylinder arrays. ITU-WAVE panel code is validated against analytical results before applied to power absorption from ocean waves for different array configurations. The effects of the separation distances between array system and heading angles on energy absorption in both sway and heave modes are studied by the support of numerical simulations which show more power absorbed in sway mode than in heave mode and sway mode has wider bandwidth than heave mode for energy absorption. It is also shown wave interactions are stronger when the array systems are close and these wave interactions are reduced significantly and shifted to larger times when the separation distance is increased. The wave interaction is much stronger at the same separation distance and heading angle in heave mode than in sway mode. Numerical experience shows that more power is absorbed in sway mode than heave mode in both two and four array systems at any separation distances and heading angles when the bodies in array system have the same displacement in both sway and heave modes.

Keywords: time domain, transient free-surface Green function, boundary integral equation, absorbed power, relative capture width, array interaction, interaction factor, truncated vertical cylinder

1. Introduction

The current development pace of wave energy converters indicates the possibility of the deployment of these converters as arrays at commercial scale. The accurate predictions of wave loads, motion characteristics, and power requirements are of critically important for the design of these devices which are in sufficiently close proximity to experience significant hydrodynamic interactions. The oscillation of each body radiates waves assuming that other bodies are not present. Some of these radiated waves interact with other bodies which can be considered as incident waves and wave diffraction occurs as the consequences while some others radiate to infinity. The response of the fluid between arrays can affect overall power generation which could increase or decrease power generation compared to isolated device. The power generation due to hydrodynamic interaction depends on separation distance, geometrical layout, direction of the incident wave, geometry in the array, incident wave length, mooring configurations, control strategies etc.

The pioneer work of Budal (1977) on wave energy converter arrays introduced the point absorber approximation in which the response amplitude are considered as equal for all devices and optimal power absorption are independent from device geometry. Besides, the characteristic dimensions (e.g. diameter) of the devices are considered small in terms of incident wave length. This approximation implicitly means that wave diffraction is not significant and can be ignored (Thomas Evans 1981, Falnes 1984). In these studies, the overall absorbed power increase or decrease are measured by interaction factor q-factor ($q > 1$ is for power increase and $q < 1$ is for power decrease) which is the ratio of power from an array to N times power from an isolated device. This q-factor is used to optimize the array layout in order to get maximum power (Fitzgerald and Thomas 2007). One of the important finding from this work was that the average value of q-factor is unity when overall heading is taken into account. This

implicitly means the power absorption is constructive in some headings while the power absorption is destructive in other headings (Wolgamot et.al. 2012).

The restriction of point absorber approximation related to diffraction waves was removed by the use of plane wave analysis in which interaction of diverging waves considered as plane waves between devices are taken into account while the near-field wave (or evanescent waves) effects are ignored implying separation distance between devices are large relative to wavelength (Spring and Monkmeyer 1974, Simon 1982, McIver and Evans 1984). The restriction on separation distance between devices or exclusion of near-field waves was overcome by the use of multiple scattering method in which the superposition of incident wave potential, diverging and near-field waves, and radiated wave by devices. In this way, the wave field around devices can be represented exactly (Ohkusu 1972, 1974, Mavrakos et.al. 2004). As the accurate solution requires high number of diffracted and radiated wave superposition with iteration, this process increases the computational time significantly (Linton and McIver 2001).

The restriction on the computational time was avoided by the use of the direct matrix method in which the multiple scattering prediction are combined with a direct approximation (Kagemoto and Yue 1986) and unknown wave amplitudes are predicted simultaneously rather than iteratively. As the numerical results of this approach which is exact depending on infinite summation truncation were very accurate compared to other numerical approximations, this method was applied to many different engineering problems including near trapping problem in large arrays (Maniar and Newman 1997), very large floating structures (Kagemoto and Yue 1993, Kashiwagi 2000), tension-leg-platforms (Yilmaz 1998), wave energy converters (Child and Venugopal 2007).

In addition to above exact formulations, the numerical tools to predict hydrodynamic interactions for multi-bodies are studied extensively by many researchers including van't Veer and Siregar (1995) who used the strip theory in which the hydrodynamic interaction s are considered as two-dimensional flow. The unified theory was used to overcome the low frequency limitations of strip theory (Breit and Sclavounos 1986, Ronaess 2002). These two-dimensional approaches give poor predictions as the hydrodynamic interactions including separation distances between the bodies are neglected in the calculations.

As the hydrodynamic interactions are inherently three-dimensional, three-dimensional numerical approximations need to be used for accurate prediction of the wave loads and motions over multi-hulls as three-dimensional effects play a significant role in the dissipation of wave energy between hulls. The hydrodynamic interactions effects are automatically taken into account as each discretized panel would have its influence on all other panels in three-dimensional numerical models. The viscous Computational Fluid Dynamics (CFD) methods for full fluid domain or viscous CFD in the near field and inviscid CFD in the far field can be used for the prediction of three-dimensional non-linear flow field due to incident waves. However, the required computational time to solve these kinds of problems is not suited for practical purposes yet.

An alternative approach to a viscous solution is the three-dimensional potential flow approximation to solve the hydrodynamic interactions. The computational time of potential (or inviscid CFD) which neglect the viscous effect is much less than viscous CFD and are used to predict the hydrodynamic loads over floating mono and multi bodies. The prediction of three-dimensional hydrodynamic interaction effects for multi bodies can be obtained using three-dimensional frequency and time domain approaches and two kinds of formulations were used for this purpose. These are Green's function

formulation (Liapis 1986, King 1987, Kara 2000) and Rankine type source distribution (Betram 1990, Nakos et.al. 1990, Xiang and Faltinsen 2011).

The Green function's approach satisfies the free surface boundary condition and condition at infinity automatically, and only the body surface needs to be discretized with panels, while the source and dipole singularities are distributed discretizing both the body surface and a portion of the free surface in Rankine type formulation. The main disadvantage of Rankine type source distribution is the stability problem for the numerical implementation, since the radiation condition or condition at infinity is not satisfied exactly. The requirement of the discretization of some portion of the free surface using quadrilateral or triangular elements increases the computational time substantially. The time domain and frequency domain results are related by the Fourier Transform in the context of the linear theory.

WAMIT (2012) is a commercial programme and uses frequency domain Green function to predict hydrodynamics loads over mono and multi bodies and used by many researcher for many different purposes including optimizing the damping characteristics of wave energy converters in the arrays, increasing the capture width of a line absorber with cylindrical floats, analysing the motions of a floating platform with several absorber attached (Bellew et.al. 2009, Stansby et.al. 2015). Other non-commercial three-dimensional frequency domain Green function approach is used by many other researchers to predict the effects of hydrodynamic interactions on absorbed power, captured with, separation distances, directionality, interaction factors, efficiency of the method in the case of large number of wave energy converters in the array, optimum control (Justino and Clement 2003, Borgarino et.al. 2012).

In the present paper, two and four truncated vertical cylinders in both sway and heave modes as a wave energy converter will be used to predict the absorbed energy from ocean waves. The time dependent hydrodynamic radiation and exciting forces impulse response functions (which are used for the time marching of the equation of motion in order to find displacement, velocity, and acceleration of the wave energy converter) are predicted by the use of the transient free-surface wave Green function (Kara and Kara et.al. 2000-2017). The present ITU-WAVE numerical results for array systems will be validated with analytical results. The effects of the separation distances and heading angles on relative capture width and interaction factor are studied in order to determine the maximum absorbed power from ocean waves and the constructive and destructive effects.

2. Equation of motion of arrays

A right-handed coordinate system is used to define the fluid action and a Cartesian coordinate system $\vec{x} = (x, y, z)$ is fixed to the body which is used for the solution of the linearized problem in the time domain Fig. 1. Positive x-direction is towards the forward, positive z-direction points upwards, and the z=0 plane (or xy-plane) is coincident with calm water. The bodies undergo oscillatory motion about their mean positions due to incident wave field. The origin of the body-fixed coordinate system $\vec{x} = (x, y, z)$ is located at the centre of the xy plane. The solution domain consists of the fluid bounded by the free surface $S_f(t)$, the body surface $S_b(t)$, and the boundary surface at infinity S_∞ Fig. 1 (Kara 2000).

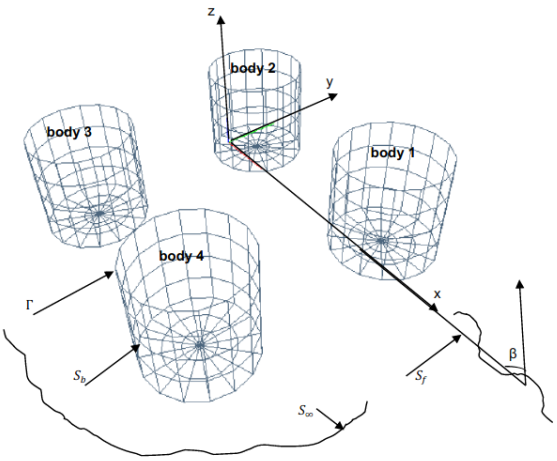

Fig. 1: Coordinate system and surface of the wave energy converters

The following assumptions are taken into account in order to solve the physical problem. If the fluid is unbounded (except for the submerged portion of the body on the free surface), ideal (inviscid and incompressible), and its flow is irrotational (no fluid separation and lifting effect), the principle of mass conservation dictates the total disturbance velocity potential $\Phi(\vec{x},t)$. This velocity potential is harmonic in the fluid domain and is governed by Laplace equation everywhere in the fluid domain as $\nabla^2\Phi(\vec{x},t) = 0$ and the disturbance flow velocity field $\vec{V}(\vec{x},t)$ may then be described as the gradient of the potential $\Phi(\vec{x},t)$ (e.g. $\vec{V}(\vec{x},t) = \nabla\Phi(\vec{x},t)$).

The dynamics of a floating body's unsteady oscillations are governed by a balance between the inertia of the floating body and the external forces acting upon it. This balance is complicated by the existence of radiated waves which results from due to the oscillations of the bodies and the scattering of the incident waves. This means that waves generated by the floating bodies at any given time will persist indefinitely and the waves of all frequencies will be generated on the free surface. These generated waves, in principle, affect the fluid pressure field and hence the body force of the floating bodies at all subsequent times. This situation introduces memory effects and is described mathematically by a convolution integral. Having assumed that the system is linear, the equation of motion of any floating bodies may be written in a form (Cummins 1962)

$$\sum_{k=1}^{6}\left(M_{kk_i}+a_{kk_i}\right)\ddot{x}_{k_i}(t)+\left(b_{kk_i}+B_{PTO-kk_i}\right)\dot{x}_{k_i}(t)+\left(C_{kk_i}+c_{kk_i}+C_{PTO-kk_i}\right)x_{k_i}(t)+\int_0^t d\tau K_{kk_i}(t-\tau)\dot{x}_{k_i}(\tau)=\int_{-\infty}^{\infty}d\tau K_{kD_i}(t-\tau)\zeta(\tau) \quad (1)$$

where $i = 1,2,3,\dots,N$ is the N number of body in the array systems. $k = 1,2,3,\dots,6$ represents six-rigid body modes of surge, sway, heave, roll, pitch, and yaw, respectively. The displacement of the floating bodies from its mean position in each of its rigid-body modes of motion is given $x_k(t) = (1,2,3,\dots,N)^T$, N is the number of wave energy converters in the array, and the over-dots indicates differentiation with respect to time. $\ddot{x}_k(t)$ and $\dot{x}_k(t)$ are acceleration and velocity, respectively. M_{kk} inertia matrix of the floating body and C_{kk} linearized hydrostatic restoring force coefficients. As the same floating body is used in the array the elements of both mass and restoring coefficients equal to each other for each body $m_1 = m_2 = \cdots = m_N = m$ and $C_1 = C_2 = \cdots = C_N = C$, respectively. m and C are the mass and restoring coefficient for mono-hull, respectively.

$$M_{kk} = \begin{pmatrix} m_1 & \cdots & 0 \\ \vdots & \ddots & \vdots \\ 0 & \cdots & m_N \end{pmatrix} \; C_{kk} = \begin{pmatrix} C_1 & \cdots & 0 \\ \vdots & \ddots & \vdots \\ 0 & \cdots & C_N \end{pmatrix} \quad (2)$$

The radiation impulse response function $K_{kk}(t)$ is the force on the j-th body due to an impulsive velocity in the k-th body. The coefficients a_{kk}, b_{kk}, and c_{kk} accounts for the instantaneous forces proportional to the acceleration, velocity, and displacement, respectively. The memory function $K_{kk}(t)$ accounts for the free surface effects which persist after the motion occurs. For the radiation problem the term 'memory function' is used to distinguish this portion of the impulse-response function from the instantaneous force components outside of the convolution on the left-hand side of Eq. (1). The coefficient a_{kk} is the time and frequency independent constant, it depends on the body geometry and is related to added mass. The coefficients b_{kk} and c_{kk} are the time and frequency independent constants and depend on the body geometry and forward speed and are related to damping and hydrostatic restoring coefficient, respectively. The memory coefficient $K_{kk}(t)$ is the time dependent part and depends on body geometry, forward speed, and time. It contains the memory effect of the fluid response. The convolution integral on the left-hand side of Eq. (1), whose kernel is a product of the radiation impulse response function $K_{kk}(t)$ and velocity of the floating body $\dot{x}_k(t)$, is a consequence of the radiated wave of the floating body. When this wave is generated, it affects the floating body at each successive time step (Ogilvie 1964).

$$K_{kk}(t) = \begin{pmatrix} K_{11} & \cdots & K_{1N} \\ \vdots & \ddots & \vdots \\ K_{N1} & \cdots & K_{NN} \end{pmatrix}, a_{kk} = \begin{pmatrix} a_{11} & \cdots & a_{1N} \\ \vdots & \ddots & \vdots \\ a_{N1} & \cdots & a_{NN} \end{pmatrix}, b_{kk} = \begin{pmatrix} b_{11} & \cdots & b_{1N} \\ \vdots & \ddots & \vdots \\ b_{N1} & \cdots & b_{NN} \end{pmatrix}, c_{kk} = \begin{pmatrix} c_{11} & \cdots & c_{1N} \\ \vdots & \ddots & \vdots \\ c_{N1} & \cdots & c_{NN} \end{pmatrix} \quad (3)$$

The term $K_{kD}(t) = (K_{1D}, K_{2D}, K_{3D}, \dots, K_{ND})^T$ on the right-hand side of Eq. (1) are the components of the exciting force and moment's impulse response functions including Froude-Krylov and diffraction due to the incident wave elevation $\zeta(t)$ which is the arbitrary wave elevation and defined at the origin of the coordinate system Fig. 1 in the body-fixed coordinate system. The kernel $K_{kD}(t)$ is the diffraction impulse response function; the force on the k-th body due to a uni-directional impulsive wave elevation with a heading angle of β.

B_{PTO-kk} and C_{PTO-kk} are time independent and frequency dependent Power-Take-Off (PTO) damping and restoring coefficient matrices for each mode of motion, respectively. The diagonal elements of B_{PTO-kk} is taken as the damping coefficient of the mono-hull at natural frequency of each mode $B_{PTO} = B_{mono}(\omega_n)$ in order to absorb maximum power (Falnes 2002) while the off-diagonal terms are considered as zero for simplicity. The elements of C_{PTO-kk} is considered as zero for heave mode while for the sway mode, the diagonal elements of C_{PTO-kk} are taken as hydrostatic restoring coefficient of heave mode in order to have the same natural frequency and displacement in both heave and sway modes. In this case, it would be possible to compare heave and surge motions and power variables directly in order to decide which mode of motion are more beneficial for power absorption.

$$B_{PTO-kk} = \begin{pmatrix} B_{mono}(\omega_n) & \cdots & 0 \\ \vdots & \ddots & \vdots \\ 0 & \cdots & B_{mono}(\omega_n) \end{pmatrix} \; C_{PTO-kk} = \begin{pmatrix} C_1 & \cdots & 0 \\ \vdots & \ddots & \vdots \\ 0 & \cdots & C_N \end{pmatrix} \quad (4)$$

Once the stiffness matrix, inertia matrix, and fluid forces e.g. radiation and diffraction forces are known, the equation of motion of floating body Eq. (1) may be time marched using the fourth-order Runge-Kutta method.

3. ITU-WAVE

The hydrodynamics functions in the present paper are predicted with in-house ITU-WAVE three-dimensional direct time domain numerical code. ITU-WAVE coded using C++ was validated against experimental, analytical, and other published numerical results (Kara and Kara et.al. 2000-2017) and used to predict the seakeeping characteristics (e.g. radiation and diffraction), resistance, added-resistance, hydroelasticity of the floating bodies, wave power absorption from ocean waves with latching control. The fluid boundaries described by the use of Boundary Integral Equation Methods (BIEM) with Neumann-Kelvin linearization in the context of potential theory.

The exact initial boundary value problem is then linearized using the free stream as a basis flow and replaced by the boundary integral equation applying Green theorem over three-dimensional transient free surface Green function. The resultant boundary integral equation is discretized using quadrilateral elements over which the value of the potential is assumed to be constant and solved using the trapezoidal rule to integrate the memory part of the transient free surface Green function in time. The free surface and body boundary conditions are linearized on the discretized collocation points over each quadrilateral element to obtain algebraic equation.

4. Comparison with analytical results

The present ITU-WAVE numerical results are compared with the analytical results of two and four truncated vertical cylinders (Kagemoto and Yue 1986) in order to validate the present numerical predictions.

4.1. Two truncated vertical cylinder arrays

Two truncated vertical cylinder Fig. 2 is used for numerical analysis as a first test case. It is assumed two cylinders have the same draft and radius R although present method can be applied for different draft and radius. The truncated cylinders have the radius of R, draft of 2R and hull separation to diameter ratio of d/D=1.3. It is assumed that two truncated cylinders are free for sway and heave modes and fixed for other modes. These two truncated cylinders are studied to predict sway and heave radiation and diffraction impulse response functions in time and added-mass, damping coefficients, and exciting forces in frequency domain. The time domain and frequency domain results are related to each other through Fourier transforms in the context of linear analysis. The present ITU-WAVE numerical results for sway and heave added-mass and damping coefficients and exciting forces (which are the sum of the diffraction and Froude-Krylov forces) with heading angle $\beta = 90^0$ are compared with the analytical results of Kagemoto and Yue (1986).

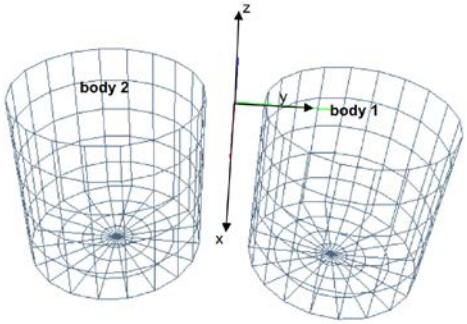

Fig. 2: Two truncated vertical cylinder with d/D=1.3

Fig. 3 shows the convergence test of radiation and diffraction impulse response functions for sway and heave modes. As two truncated vertical cylinder is symmetric in terms of xz-coordinate plane of the reference coordinate system, only single hull form is discretized for numerical analysis. Numerical experience showed that numerical results are not very sensitive in terms of non-dimensional time step size $t * sqrt(g/L)$ of 0.01, 0.03, and 0.05 over the range of panel numbers of 96, 150, 216, 294 on single body of two truncated vertical cylinder whilst the numerical results are quite sensitive in terms of panel numbers as can be seen in Fig. 2 and the results at panel number 216 on single hull form is converged and used for the present ITU-WAVE numerical calculations for both two and single truncated vertical cylinder with the non-dimensional time step size of 0.05.

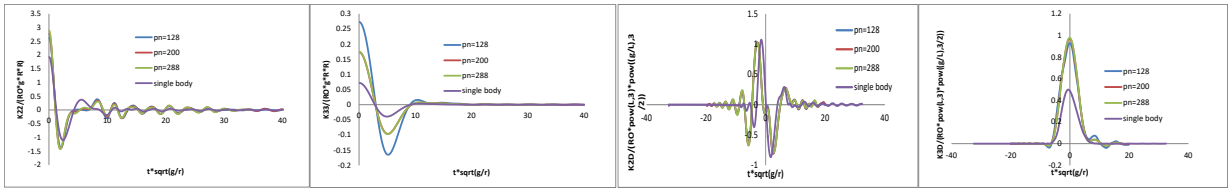

Fig. 3: Two truncated vertical cylinder with d/D=1.3, non-dimensional radiation $K_{22}(t)$ and $K_{33}(t)$ and diffraction sway and heave $K_{2D}(t)$ and $K_{3D}(t)$ impulse response functions at beam seas $\beta = 90^0$

It may be noticed that the magnitude of radiation Impulse Response Functions (IRF) of two cylinder in heave mode Fig. 3 is approximately twice of IRF of single cylinder while it is less than double in the case of sway mode. The other distinctive difference of IRF of single and two cylinders in Fig. 3 is the behaviour of these IRFs functions in longer times in sway mode. IRFs of two cylinders have oscillations over longer times with decreasing amplitude in sway mode while single cylinder IRF decays to zero just after first oscillation. This behaviour of IRF implicitly means that the energy between two cylinders is trapped in the gap and only a minor part of the energy is radiated outwards each time the wave is reflected off the hull while all energy is dissipated in the case of single cylinder in sway mode and in both two and single cylinders in heave mode. It is expected that geometry of two bodies would significantly affects the radiated, diffracted, and trapped waves which result from due to standing waves in the gap. In the case of diffraction IRF in Fig.3, there are no significant differences in sway mode between single and two cylinders' IRFs whilst it is doubled in heave mode.

The time dependent radiation and exciting IRFs in time domain are related to the frequency dependent added-mass and damping coefficients and force amplitude, respectively in frequency domain through Fourier transforms when the motion is considered as a time harmonic motion. Added-mass $A_{22}(\omega)$ and $A_{33}(\omega)$, damping coefficients $B_{22}(\omega)$ in Fig. 4 and exciting forces amplitudes $F_2(\omega)$ and $F_3(\omega)$ in Fig. 5 is obtained by the Fourier transform of radiation sway IRF $K_{22}(t)$ and radiation heave IRF $K_{33}(t)$ of Fig. 3, and diffraction sway IRF $K_{2D}(t)$ and diffraction heave IRF $K_{3D}(t)$ of Fig. 3, respectively.

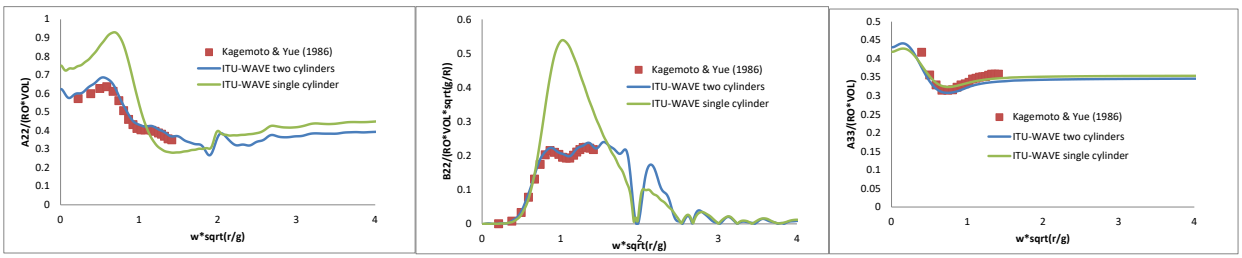

Fig. 4: Two truncated vertical cylinders with d/D=1.3, non-dimensional sway and heave added-mass and damping coefficients.

ITU-WAVE numerical results of added-mass and damping coefficients in sway mode and added-mass coefficients in heave mode of two cylinders are satisfactory agreement with the analytical prediction of Kagemoto and Yue (1985) as can be seen in Fig. 4. In addition to two cylinders added-mas and damping coefficients in Fig. 4, the single cylinder results are presented as the comparison with two cylinders results. It can be seen in Fig. 4 the behaviours of two cylinders results in sway mode are significantly different from those of single cylinder due to trapped waves and hydrodynamic interactions in the gap of two cylinders whilst in heave mode single and two cylinders added-mass result does not show such difference as most of the energy is dissipated in this mode.

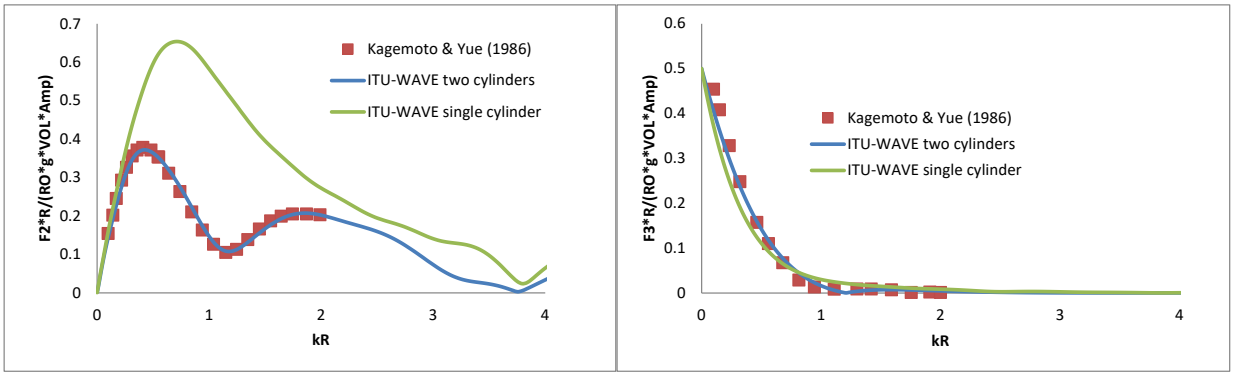

Fig. 5: Two truncated vertical cylinders with d/D=1.3, non-dimensional sway and heave exciting force amplitude at beam seas $\beta = 90^0$.

The effects of diffraction hydrodynamic interactions in sway mode (at which interactions are effective in the whole frequency range) are much stronger than in heave mode as can be observed in Fig. 5. This interaction effects in sway mode are even stronger in a limited frequency range which is of interest for the motions of the bodies in array systems and is around kR =0.5 and kR = 2.0 of non-dimensional frequency in radiation and diffraction sway mode in Fig. 5.

4.2. Four truncated vertical cylinder arrays

Four truncated vertical cylinder Fig. 1 is used for numerical analysis as the second test case. As in two cylinders, it is assumed four cylinders have the same draft and radius. Four truncated cylinders have the radius of R and draft of 2R and hull separation to diameter ratio of d/D=2.0. It is assumed that four truncated cylinders are free for sway mode and fixed for other modes and are studied to predict sway radiation and diffraction impulse response functions in time and added-mass, damping coefficients, and exciting forces in frequency domain. The present ITU-WAVE numerical results for sway added-mass and damping coefficients and exciting forces with heading angle $\beta = 90^0$ are compared with the analytical results of Kagemoto and Yue (1986).

Fig. 6 shows the convergence test of radiation and diffraction impulse response functions for sway mode. As four truncated vertical cylinders are symmetric, only single hull form is discretized for numerical analysis. Numerical experience showed that numerical results at panel number 200 on single hull form is converged and used for the present ITU-WAVE numerical calculations for both four and single truncated vertical cylinder with the non-dimensional time step size of 0.05.

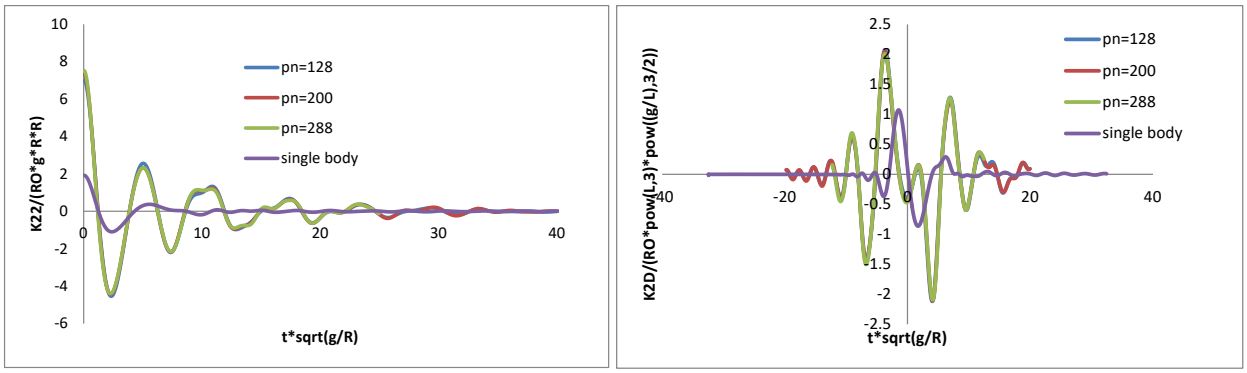

Fig. 6: Four truncated vertical cylinder with d/D=2.0, non-dimensional radiation $K_{22}(t)$ and diffraction $K_{2D}(t)$ sway impulse response functions at beam seas $\beta = 90^0$

When the two (Fig. 3) and and four (Fig. 6) truncated vertical cylinders' radiation IRFs are compared, it can be observed that the amplitude of radiation IRFs of four truncated cylinders are approximately 2.5 times higher than two cylinders' radiation IRFs and four cylinders' IRFs have oscillations over longer times with decreasing amplitude in sway mode compared to cylinders' IRFs. This behaviour implicitly means that more energy capture between bodies in four cylinders than two cylinders. The same outcome is valid for diffraction IRFs too.

Fig. 7 shows added-mass $A_{22}(\omega)$, damping coefficients $B_{22}(\omega)$ and exciting forces amplitudes $F_2(\omega)$ which are obtained by the Fourier transform of radiation sway IRF $K_{22}(t)$ of Fig. 6, and diffraction sway IRF $K_{2D}(t)$ of Fig. 6, respectively. ITU-WAVE numerical results of four cylinders are satisfactory agreement with those of Kagemoto and Yue (1985) as can be seen in Fig. 7.

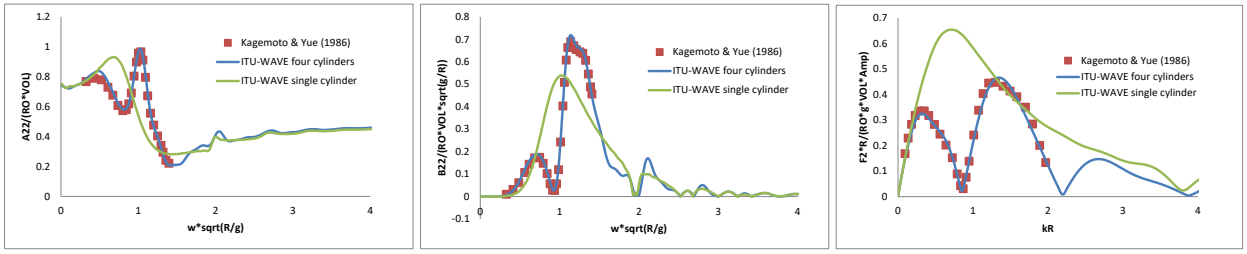

Fig. 7: Four truncated vertical cylinders with d/D=2.0, non-dimensional sway added-mass, damping, and exciting force amplitude at beam seas $\beta = 90^0$.

There would not be energy transfer or radiated waves from floating body to sea when the damping coefficients are zero as can be observed in Fig. 7. It may be noticed there are three resonance resonances behaviours in damping coefficients in sway mode which implies that high standing waves occur between the maximum and minimum damping coefficients (van Oortmersen (1979), Ohkusu (1969)). It may be noticed the peaks are finite at non-dimensional resonance frequencies as some of the wave energy dissipate under the floating body and radiates to the far field.

5. The interactions of bodies in array system

The radiation impulse response functions (IRF) for sway and heave modes in the case of two interacting bodies are presented for the range of different separation distances in Fig. 8. IRFs K12 (t) which represents the interactions between two truncated vertical cylinders is very strong and the same order with K11 (t), whilst the interactions become weaker as the separation distance between interacting

bodies are increased. The interactions IRFs on body 1 and body 2 have the same magnitude and sign as it is presented in Fig. 8. Giving one body an impulsive velocity in one mode causes a force in the same mode on the other body after some finite time t, which is the time it takes the wave to move the distance between bodies. This means that energy is trapped in the gap between bodies, only a minor part of the energy is radiated outwards each time the wave is reflected off the body.

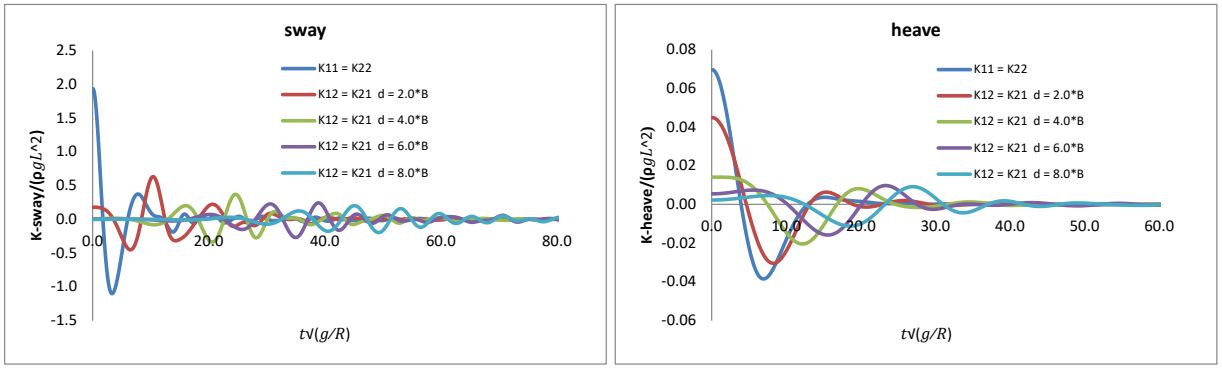

Fig. 8: Two truncated vertical cylinders with the range of different separation distances, non-dimensional radiation sway and heave Impulse Response Functions (IRFs).

It may be noticed from Fig. 8 the dominant part of the interactions between these two vertical cylinder are shifted to the larger times as the separation distances increase. The exciting force IRFs (which are the sum of diffraction and Froude-Krylov forces) for sway and heave modes are presented in Fig. 9 for the range of different separation distances at heading angle $\beta = 90^0$.

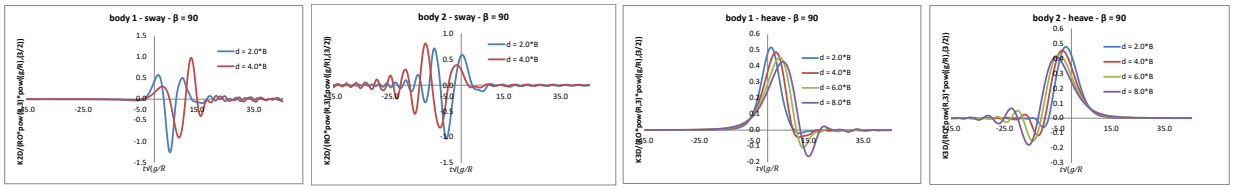

Fig. 9: Two truncated vertical cylinders with the range of different separation distances, non-dimensional exciting sway and heave IRFs at beam seas $\beta = 90^0$.

It may be noticed from Fig. 9 when the separation distances increase, the interaction between incident wave and the first body which interact with the incident wave first is delayed for longer times, whilst it is contrary for the second body which in the wake of the first body in the case of heading angle $\beta = 90^0$.

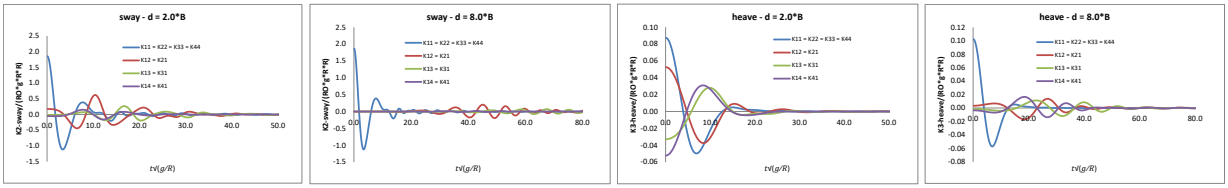

Fig. 10: Four truncated vertical cylinders with d = 2.0*B and d = 8.0*B separation distances, non-dimensional radiation sway and heave Impulse Response Functions (IRFs).

Radiation IRFs of sway and heave modes for four truncated vertical cylinder ae presented in Fig. 10 for the separation distance of 2.0*B and 8.0*B in order to predict the interaction of bodies in the array. As in two truncated, in the case of small separation distance of 2.0*B, the interaction between the bodies

are quite significant while the interaction effect decrease for larger separation distance of 8.0*B and the maximum response amplitude shifted to larger times.

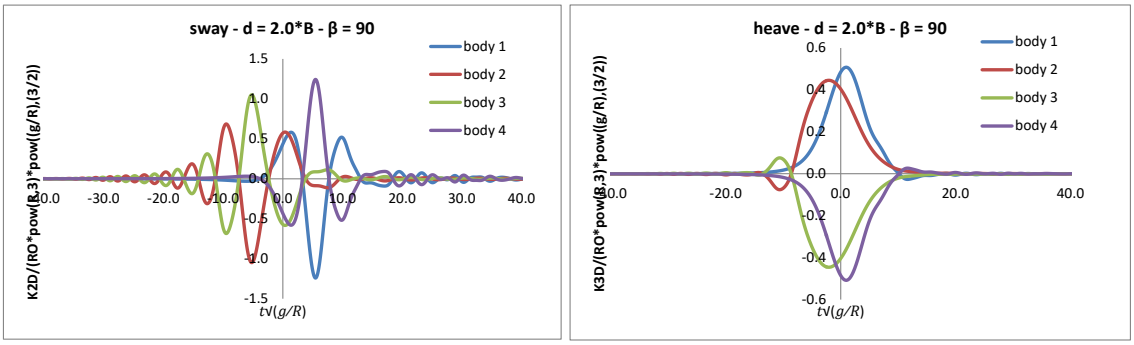

Fig. 11: Four truncated vertical cylinders with the range of different separation distances, non-dimensional exciting sway and heave IRFs at beam seas $\beta = 90^0$.

Exciting sway and heave IRFs for four truncated cylinder at beam seas $\beta = 90^0$ and separation distance of d = 2.0*B are presented in Fig. 11. It may be noticed in Fig. 11 the exciting forces on body 1 and body 4 which is on the wake of body 1 as well as on body 2 and body 3 which is on the wake of body 2 have the same magnitudes but opposite signs. This is the numerical prediction that is expected as the truncated four cylinder are symmetric both in x- and y-directions. The wave is reflected off the bodies and translating across the gap between hulls to hit the other body.

6. Response Amplitude Operators (RAOs) in sway and heave modes

As sway mode does not have restoring coefficient, PTO restoring coefficient of the truncated circular cylinder are taken as hydrostatic restoring coefficient of heave mode in order to have the same natural frequency and displacement in both heave and sway modes as indicated above. RAOs of two and four truncated vertical cylinder in sway and heave modes at beam seas $\beta = 90^0$ are presented in Fig. 12. RAOs are taken by the use of Eq. (1) after time simulation of equation of motion achieving the steady state condition at the range of the different frequencies.

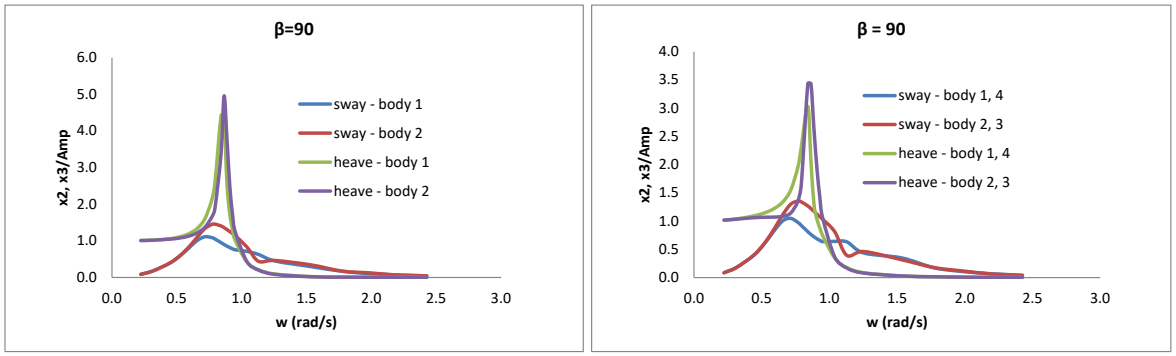

Fig. 12: Two (right) and four (left) truncated vertical cylinders, sway and heave motions RAOs at beam seas $\beta = 90^0$.

It may be noticed that the motion of the second body which is at the wake of the first body at beam seas $\beta = 90^0$ in the case of two bodies Fig.2 and that of the second and third bodies which are at the wake of the first and fourth bodies, respectively in the case of four truncated cylinder Fig. 1 is higher around resonance frequency in both sway and heave modes. This is mainly due to the trapped waves between

hulls. In the case of four truncated vertical cylinder Fig. 1, it may also be noticed that the motion of the first and fourth body in the array system and the second and third body is exactly the same which is due to symmetry in terms of x- and y- coordinate systems Fig. 1.

The heave motion amplitude in resonance frequency is more than two times of sway motion amplitude around resonance frequency. This is mainly due to the damping coefficients as sway mode damping coefficients are much bigger than heave damping coefficients around resonance frequency. As the motion is controlled by the damping coefficients around the resonance frequency and sway mode have much bigger damping coefficients, the sway motion is damped around resonance frequency compared to heave motion. However, the sway motion distributed wider frequency range as heave motion mainly concentrated at resonance frequency.

7. Instantaneous and mean absorbed power

The instantaneous power $P_{ins_{k_i}}(t)$ absorbed by Power-Take-Off (PTO) system for each body in the array is directly proportional to exciting (which is the sum of diffraction and Froude-Krylov forces) and radiation forces on WEC and is defined as

$$P_{ins_{k_i}}(t) = [F_{exc_{k_i}}(t) - F_{rad_{k_i}}(t)] \cdot \dot{x}_{k_i}(t) \qquad (5)$$

where $F_{exc_i}(t)$ exciting forces which are due to incident and diffracted waves, $F_{rad_i}(t)$ radiation forces which are due to the oscillation of WEC. $F_{exc_i}(t)$ and $F_{rad_i}(t)$ are given as in Eq. (1)

$$F_{exc_{k_i}}(t) = F_{k_i}(t) = \int_{-\infty}^{\infty} d\tau K_{kD_i}(t-\tau)\zeta(\tau) \quad (6)$$

$$F_{rad_{k_i}}(t) = F_{kk_i}(t) = -a_{kk_i}\ddot{x}_{k_i}(t) - b_{kk_i}\dot{x}_{k_i}(t) - c_{kk_i}x_{k_i}(t) - \int_0^t d\tau K_{kk_i}(t-\tau)\dot{x}_{k_i}(\tau) \quad (7)$$

The power due to exciting forces $P_{exc_{k_i}}(t) = F_{exc_{k_i}}(t) \cdot \dot{x}_{k_i}(t)$ are the total absorbed power from the incident and diffracted waves, whilst the power due to radiation forces $P_{rad_{k_i}}(t) = -F_{rad_{k_i}}(t) \cdot \dot{x}_{k_i}(t)$ are the power radiated back to sea due to the oscillation of the WEC. The mean (average) power $\bar{P}_{ins_{k_i}}(t)$ absorbed by the PTO system over a time range T is given by

$$\bar{P}_{ins_{k_i}}(t) = \frac{1}{T}\int_0^T dt \cdot [F_{exc_{k_i}}(t) - F_{rad_{k_i}}(t)] \cdot \dot{x}_{k_i}(t) \quad (8)$$

The averaging time T must be much larger than the characteristics period of the incident wave which is approximately from 5s to 15s. In order to avoid the transient effects, only the last half of the time domain results are taken into account for the prediction of the mean absorbed power using Eq. (8) and other time dependent parameters. The total mean absorbed power $\bar{P}_{T_k}(t)$ for N number of array systems and for mode k is given as

$$\bar{P}_{T_k}(t) = \sum_{i=1}^{N} \bar{P}_{ins_{k_i}}(t) \qquad (9)$$

The total absorbed power with two and four truncated vertical cylinders in sway and heave modes at heading angle $\beta = 90^0$ and separation distance d = 4.0*B are presented in Fig.12 using asymptotic value of Eq. (9).

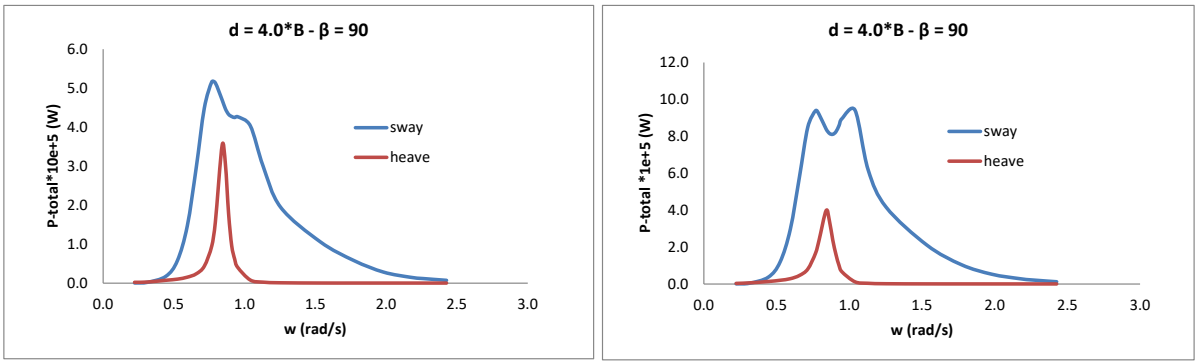

Fig. 12: Two (right) and four (left) truncated vertical cylinders, sway and heave total power at separation distance d = 4.0*B and beam seas $\beta = 90^0$.

The power absorption is concentrated around the resonance frequency in heave mode whilst power absorption has wider frequency range and the frequency bandwidth of power absorption is much larger in sway mode than heave mode. It may be noticed that power absorption are doubled in sway mode as number of WEC increased from two to four whilst absorbed power is not changed in the case of heave mode.

8. Capture width and relative capture width

A good wave energy converter is a converter which absorbs as much energy as possible from the incident wave. However, to absorb maximum power, the body must interact with the sea significantly, (i.e. the characteristic frequencies of the incident waves must be close to the resonance frequency of the body). The quantity employed to evaluate the performance of a device in term of power absorption is the capture width. At a given frequency, it is the ratio between the total mean power absorbed and the mean power per unit crest wave width of the incident wave train. The capture width $l_{cw_{k_i}}(\omega)$ for each incident wave frequency ω, for each mode k, and for a body i in array systems is defined as [Budal Falnes 1976]

$$l_{cw_{k_i}}(\omega) = \frac{\bar{P}_{ins_{k_i}}(\omega)}{P_w(\omega)} \qquad (10)$$

where $\bar{P}_{ins_{k_i}}(\omega)$ is the mean absorbed power and is obtained as the asymptotic value of the mean of the instantaneous power Eq. (8), $P_w(\omega) = \rho g^2 \zeta_0^2 / 4\omega$ is the wave power in the incident wave train per unit crest length, ζ_0 being the incident wave amplitude. The maximum capture width for heave mode is $\lambda/2\pi$, whilst it is λ/π for surge or sway mode. Relative capture width is obtained by dividing capture width with width B of the wave energy converters

$$l_{rcw_{k_i}}(\omega) = l_{cw_{k_i}}(\omega)/B \quad (11)$$

If the relative capture width is greater than 1 at any incident wave frequencies, this implies that the absorbed power can be greater than the incident wave power at these frequencies.

8.1. Separation distance effect on capture width

The relative capture width of two truncated vertical cylinders at heading angle $\beta = 90^0$ in sway and heave mode are presented in Fig. 13 using Eq. (11). Relative capture width in both sway and heave modes for body 1 is less than single body at all frequency range whilst for body 2 it is contrary. This implicitly means that the wave interaction with body 1 has the destructive effects while the wave interaction has constructive effects for body 2 as wave energy trapped between hulls. This implies that the absorbed power can be greater than the incident wave power at these frequencies for body 2.

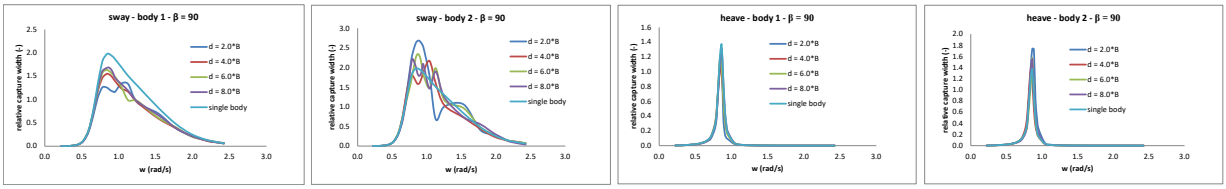

Fig. 13: Two truncated vertical cylinders, sway and heave relative capture width at beam seas $\beta = 90^0$

Due to symmetry both x- and y-directions, in the case of four truncated vertical cylinders, capture width of body 1 and body 4 is the same as well as body 2 and body 3 in Fig. 14. The capture width for four bodies in beam seas $\beta = 90^0$ using Eq. (11) is presented in Fig. 14.

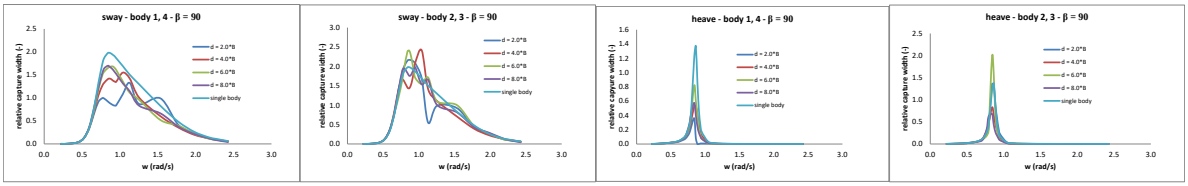

Fig. 14: Four truncated vertical cylinders, sway and heave relative capture width at beam seas $\beta = 90^0$

As in the case of two truncated cylinders in sway mode, the capture width for body 1 and body 4 has destructive effects (e.g. absorbed less power than isolated body) around resonance frequency at which most power is captured whilst body 2 and body 3 in the array system has constructive effects. It may be noticed in Fig. 14 the power is absorbed in wider frequency ranges in sway mode whilst the power is absorbed only around resonance frequency in the case of heave mode. It may also be noticed that in heave mode wave interactions have destructive effects compared to single body apart from separation distance of d = 6.0*B for body 2 and body 3.

8.2. Heading angle effect on capture width

The effect of heading angles on capture width at separation distance d = 2.0*B in both sway and heave modes are presented in Fig. 15 which shows that the maximum power absorbed in the heading angle of $\beta = 90^0$ in both sway and heave modes. When compared with heave mode which only absorbed power around resonance frequency, the bandwidth of absorbed power is larger in sway mode.

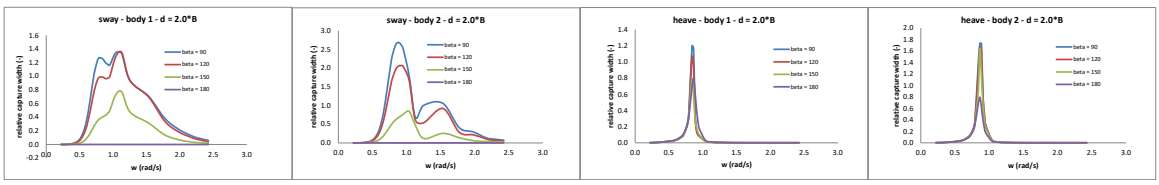

Fig. 15: Two truncated vertical cylinders, sway and heave relative capture width at separation distance d = 2.0*B and range of different heading angles

The effect of heading angles from 90 degrees to 180 degrees for four truncated vertical cylinder in both sway and heave modes are presented in Fig. 16 which shows relative capture width for separation distance d = 2.0*B.

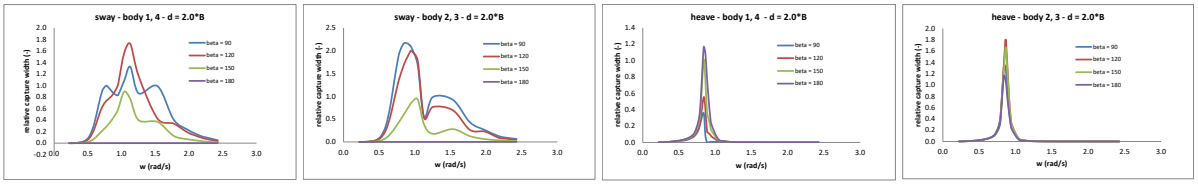

Fig. 16: Four truncated vertical cylinders, sway and heave relative capture width at separation distance d = 2.0*B and range of different heading angles

More power is absorbed from ocean waves in heading angle $\beta = 120^0$ than other heading angle in sway mode for body 1 and body 2 whilst for body 2 and body 3 almost the same level power absorbed at heading angle $\beta = 120^0$ and $\beta = 90^0$ in Fig. 16. In the case of heave mode, more power is absorbed in heading angle $\beta = 180^0$ for body 1 and body 4 whilst the heading angle $\beta = 120^0$ is the heading angle at which more power is absorbed for body 2 and body 3 in Fig. 16.

9. Interaction factor

The interaction factor due to diffracted and radiated waves gives information about the mean interactions between bodies of array systems and represents the mean gain factor for each body of the interacting systems of N bodies. Two kind of interaction factors are used in the present paper, standard $q_{k_i}(\omega)$ for a given incident wave frequency, mode k, and body i in the array system and modified $q_{mod_{k_i}}(\omega)$. The overall power production from WEC are very sensitive to the interaction factor. Depending on separation distances between bodies, geometry of WEC, control strategies, wave length, and heading angles, standard $q_{k_i}(\omega)$ factor can have constructive ($q_{k_i}(\omega) > 1$) or destructive ($q_{k_i}(\omega) < 1$) effect and given as (Thomas Evans 1981)

$$q_{k_i}(\omega) = \frac{\bar{P}_{ins_{k_i}}(\omega)}{\bar{P}_{ins_{k_0}}(\omega)} \quad (11)$$

where $\bar{P}_{ins_{k_0}}(\omega)$ is the absorbed power from an isolated WEC. The constructive ($q_{k_i}(\omega) > 1$) effect implicitly means that power absorption from array system increases in that particular wave frequency, whilst the power absorption decreases in the case of destructive ($q_{k_i}(\omega) < 1$) effect.

In the case of modified interaction factor $q_{mod_{k_i}}(\omega)$ which is given in Eq. (12), the dominant wave interaction which results in maximum power absorption in the array systems and occurs around natural frequency of WEC are taken into account and weaker wave interaction in which the power absorption is lower are filtered out from the power prediction (Babarit 2010).

$$q_{mod_{k_i}}(\omega) = \frac{\bar{P}_{ins_{k_i}}(\omega) - \bar{P}_{ins_{k_0}}(\omega)}{max_{\omega}\bar{P}_{ins_{k_0}}(\omega)} \quad (12)$$

The modified interaction factor $q_{mod_{k_i}}(\omega)$ Eq. (12) can have constructive ($q_{k_i}(\omega) > 0$) or destructive ($q_{k_i}(\omega) < 0$) effect.

9.1. Separation distance effect on interaction factor

The interaction factor $q_{k_i}(\omega)$ for sway and heave modes at heading angle $\beta = 90^0$ and different range of separation distances is presented in Fig. 17 using Eq. (11). It can be seen in Fig. 17 in both sway and heave modes for body 1 separation distance has destructive effects.

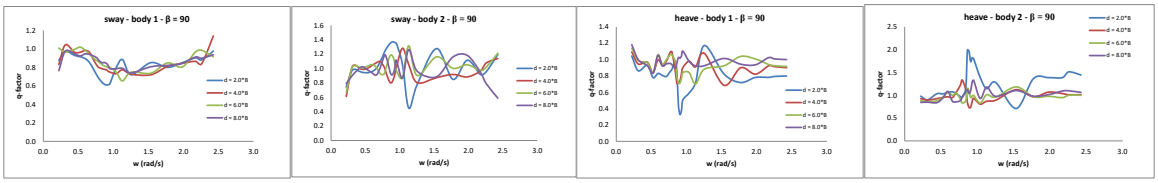

Fig. 17: Two truncated vertical cylinders, sway and heave standard interaction factor at the range of different separation distances and heading angle $\beta = 90^0$

As expected the strongest effects are due to shortest separation distance d = 2.0*B. However, for body 2 which is on the wake of the body 1, wave interactions have both constructive and destructive effects depending on incident wave frequencies.

The modified interaction factor $q_{mod_{k_i}}(\omega)$ for two truncated vertical cylinders in both sway and heave modes are presented in Fig. 18 using Eq. (12). It can be seen from Fig. 18 the effects of incident wave frequencies away from the resonance frequency are filtered out as mentioned above. This is valid for both sway and heave modes.

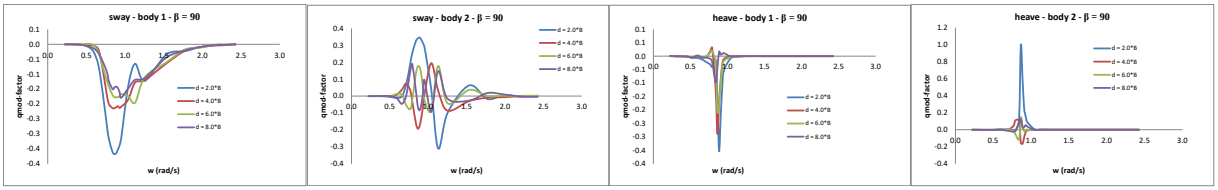

Fig. 18: Two truncated vertical cylinders, sway and heave modified interaction factor at the range of different separation distances and heading angle $\beta = 90^0$

It may be noticed in Fig. 18 for body 1 in sway and heave modes the wave interactions are destructive while for body 2 the wave interactions are both constructive and destructive depending on the wave frequency. As in the relative capture width in Fig. 13 – 16, destructive or constructive wave interaction effects have wider frequency range in sway mode compared to heave mode at which power absorption is mainly around resonance frequency as can be observed from Fig. 18.

9.2. Heading angles effect on interaction factor

The modified interaction factor $q_{mod_{k_i}}(\omega)$ Eq. (12) for two truncated vertical cylinders at separation distance d = 2.0*B and different heading angles in both sway and heave modes are presented in Fig. 19 which shows that heading angle $\beta = 150^0$ in sway mode for both body 1 and body 2 has most favourable constructive effects at different incident wave frequencies.

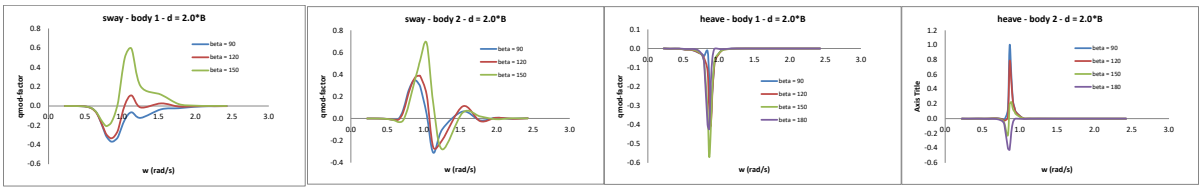

Fig. 19: Two truncated vertical cylinders, sway and heave modified interaction factor $q_{mod_{k_i}}(\omega)$ at the range of different heading angles and separation distance d = 2.0*B

In the case of heave mode at all heading angles, body 1 has destructive effect as can be seen in Fig. 19 while at heading angle $\beta = 90^0$ body 2 has maximum constructive effect compared to other heading angles.

The modified interaction factor $q_{mod_{k_i}}(\omega)$ in sway mode for four truncated vertical cylinders is presented in Fig. 20 for the separation distance d = 2.0*B and different heading angles. As in the case of two cylinders Fig. 19 in sway mode, the most favourable heading angle is $\beta = 150^0$ which has more constructive effects compared to other heading angles for all bodies in the array system.

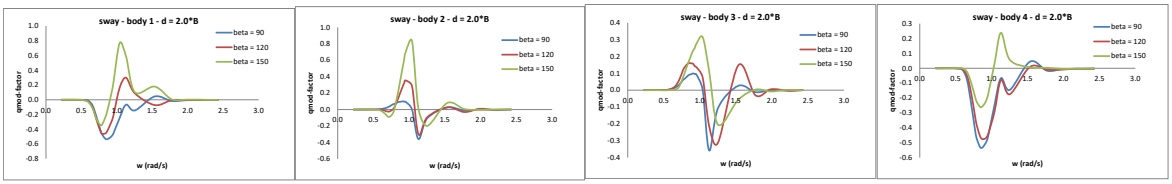

Fig. 20: Four truncated vertical cylinders, sway modified interaction factor $q_{mod_{k_i}}(\omega)$ at the range of different heading angles and separation distance d = 2.0*B

The modified interaction factor $q_{mod_{k_i}}(\omega)$ in heave mode for four truncated vertical cylinders is presented in Fig. 21 for the separation distance d = 2.0*B and different heading angles.

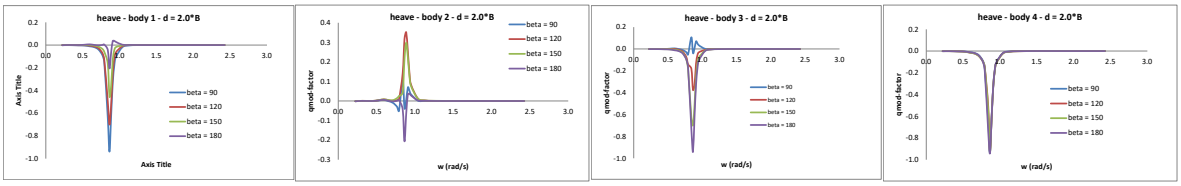

Fig. 21: Four truncated vertical cylinders, heave modified interaction factor $q_{mod_{k_i}}(\omega)$ at the range of different heading angles and separation distance d = 2.0*B

Body 1, body 3 (except heading angle $\beta = 90^0$), and body 4 in all heading angles has destructive effects in heave mode in the case of four truncated vertical cylinders as can be seen in Fig. 21 whilst body 2 in the array system has constructive effects in all heading angles except heading angle $\beta = 180^0$.

10. Conclusions

The numerical capability of present ITU-WAVE three-dimensional transient wave-structure interaction panel method is extended to predict the power absorption from ocean waves in array systems. The present numerical results in both sway and heave modes are validated with analytical results after obtain the radiation added-mass and damping coefficients as well as exciting force amplitude using Fourier transforms in order to present the results in frequency domain.

The numerical experience shows that power absorptions in sway modes in any separation distances and heading angles are much higher than in heave mode and have wider bandwidth in frequency range in sway mode. The absorbed wave power is much higher in heading angle $\beta = 150^0$ than any other heading angle in the case of sway mode in both two and four truncated vertical cylinders.

In the case of heave mode, the most effective heading angle for constructive effect for two and four truncated cylinders are mixed. The maximum constructive effect is heading angle $\beta = 90^0$ for two truncated cylinder whilst it is heading angle $\beta = 120^0$ for body 2 in the array system and is the heading angle $\beta = 90^0$ for body 3 in the case of four truncated vertical cylinder.

The numerical experience also shows that if the bodies in the array system are close the wave interactions are stronger at any wave headings and separation distances and the interaction effect is significantly diminished and maximum wave interaction when separation distance is increased. The wave interaction in heave mode is much stronger than in sway mode.

References

Babarit A. Impact of long separating distances on the energy production of two interacting wave energy converters. Ocean Engineering 2010;37(8-9):718-729.

Bellew S, Stallard T, Stansby P. Optimisation of a heterogeneous array of heaving bodies. Proceedings of the 8th European Wave and Tidal Energy Conference (EWTEC 2009) 2009;1-9.

Bertram V. Ship Motions by Rankine Source Method. Ship Technology Research 1990;37 (4):143-152.

Borgarino B, Babarit A, Ferrant P. Impact of wave interactions effects on energy absorption in large arrays of wave energy converters. Ocean Engineering 2012;41:79-88.

Budal K. Theory for absorption of wave power by a system of interacting bodies. Journal of Ship Research 1977;21(4):248-253.

Budal K, Falnes J. Optimum operation of wave power converter. Internal Report, Norwegian University of Science and Technology 1976

Breit S, Sclavounos P. Wave Interaction Between Adjacent Slender Bodies. Journal of Fluid Mechanics 1986;165:273-296.

Child BFM, Venugopal V. Interaction of waves with an array of floating wave energy devices. Proceedings of the 7th European Wave and Tidal Energy Conference (EWTEC 2007) 2007.

Cummins WE. The Impulse response function and ship motions. Shiffstechnik 1962;9:101-109.

Fitzgerald C, Thomas GP. A preliminary study on the optimal formation of an array of wave power devices. Proceedings of the 7th European Wave and Tidal Energy Conference 2007.

Justino PAP, Clement AH. Hydrodynamic performance for small arrays of submerged spheres. Proceedings of the 5th European Wave and Tidal Energy Conference (EWTEC 2003) 2003;266-273.

Kagemoto H, Yue DKP. Interactions among multiple three-dimensional bodies in water waves: an exact algebraic method. Journal of Fluid Mechanics 1986;166:189-209.

Kagemoto H, Yue DKP. Hydrodynamic interaction analyses of very large floating structures. Marine Structures 1993;6:295-322.

Kara F. Time domain hydrodynamics and hydroelastics analysis of floating bodies with forward speed. PhD thesis, University of Strathclyde 2000

Kara F, Vassalos D. Time domain prediction of steady and unsteady marine hydrodynamic problem. International Shipbuilding Progress 2003;50(4):317-332.

Kara F, Vassalos D. Time domain computation of wavemaking resistance of ships. Journal of Ship Research 2005;49 (2):144-158.

Kara F, Vassalos D. Hydroelastic analysis of cantilever plate in time domain. Ocean Engineering 2007;34:122-132.
Kara F. Time domain prediction of power absorption from ocean waves with latching control. Renewable Energy 2010;35:423-434.
Kara F. Time domain prediction of added-resistance of ships. Journal of Ship Research 2011;55 (3):163-184.
Kara F. Time domain prediction of hydroelasticity of floating bodies. Applied Ocean Research 2015;51:1-13.
Kara F. Time domain prediction of seakeeping behaviour of catamarans. International Shipbuilding Progress 2016;62 (3-4), 161-187.
Kara F. Time Domain Prediction of Power Absorption from Ocean Waves with Wave Energy Converters Arrays. Renewable Energy 2016;92, 30-46.
Kara F. Point absorber wave energy converter in regular and irregular waves with time domain analysis. International Journal of Marine Science and Ocean Technology 2016;3(7), 74-85.
Kara F. Control of wave energy converters for maximum power absorptions with time domain analysis. Journal of Fundamentals of Renewable Energy and Applications 2017; 7(1), 1-8.
Kashiwagi M. Hydrodynamic interactions among a great number of columns supporting a very flexible structure. Journal of Fluids and Structures 2000;14:1013-1034.
King BW. Time Domain Analysis of Wave Exciting Forces on Ships and Bodies. PhD thesis, The Department of Naval Architecture and Marine Engineering, The University of Michigan, Ann Arbor, Michigan, USA 1987.
Liapis S. Time Domain Analysis of Ship Motions. PhD thesis, The Department of Naval Architecture and Marine Engineering, The University of Michigan, Ann Arbor, Michigan, USA 1986.
Linton CM, McIver M. Handbook of mathematical techniques for wave-structure interactions. Chapman and Hall 2001.
Maniar HD, Newman JN. Wave diffraction by a long array of cylinders. Journal of Fluid Mechanics 1997;339:309-330.
Mavrakos SA, Katsaounis GM, Nielsen K, Lemonis G. Numerical performance investigation of an array of heaving wave power converters in front of a vertical breakwater. Proceedings of 14th international offshore and polar engineering conference (ISOPE-2004) 2004;238-245.
McIver P, Evans DV. Approximation of wave forces on cylinder arrays. Applied Ocean Engineering 1984;6(2):101-107.
Nakos D, Sclavounos PD. Ship Motions by a Three Dimensional Rankine Panel Method. Proceedings of the 18th Symposium on Naval Hydrodynamics, Ann Arbor, Michigan, USA 1990;21-41.
Ohkusu M. Wave action on groups of vertical circular cylinders. Journal of the Society of Naval Architects in Japan 1972;131.
Ohkusu M. On the heaving motion of two circular cylinders on the surface of a fluid. Reports of Research Institute for Applied Mechanics, No. 58, 1969;17:167-185
Ohkusu M. Hydrodynamics forces on multiple cylinders in waves. Proceedings of the international symposium on dynamics of marine vehicles and structures in waves 1974;107-112.
Ogilvie TF. Recent progress toward the understanding and prediction of ship motions. Proceedings of the 5th Symposium on Naval Hydrodynamics, Office of Naval Research, Washington, D.C., USA 1964;3-128.
Ronæss M. Wave induced motions of two ships advancing on parallel course. PhD thesis, Department of Marine Hydrodynamics, NTNU, Trondheim, Norway 2002.
Simon MJ. Multiple scattering in arrays of axisymmetric wave-energy devices. Part 1. A matrix method using a plane-wave approximation. Journal of Fluid Mechanics 1982;120:1-25.

Spring BH, Monkmeyer PL. Interaction of plane waves with vertical cylinders. Proceedings of 14th international conference on coastal engineering 1974;1828-1845.

Stansby P, Carpintero E, Stallard T, Maggi A. Three-float broad-band resonant line absorber with surge for wave energy conversion. Renewable Energy 2015*;78*:132-140.

Thomas GP, Evans DV. Arrays of three-dimensional wave-energy absorbers. Journal of Fluid Mechanics 1981;108:67-88.

van Oortmerssen G. Hydrodynamic interaction between two structures floating in waves. Proceedings of the 2nd International Conference on Behaviour of Offshore Structures (BOSS'79), London, UK 1979;339-356

van't Veer AP, Siregar FRT. The interaction effects on a catamaran travelling with forward speed in waves. Proceedings of 3rd International Conference of Fast Sea Transportation 1995; 87-98.

WAMIT User Manual, Version 7.0, 2012.

Wolgamot HA, Taylor PH, Taylor Eatock R. The interaction factor and directionality in wave energy arrays. Ocean Engineering 2012;47:65-73.

Yilmaz O. Hydrodynamic interactions of waves with group of truncated vertical cylinders. Journal of Waterway, Port, Coastal and Ocean Engineering 1998;124(5):272-279.

Xiang X, Faltinsen OM. Time domain simulation of two interacting ships advancing parallel in waves. Proceedings of the ASME 30th International Conference on Ocean, Offshore and Arctic Engineering, Rotherdam, The Netherlands 2011.